NUKLEONIKA 2015;60(1):103–108
doi: 10.1515/nuka-2015-0021

ORIGINAL PAPER

DE GRUYTER
OPEN

Effects of Co, Ni, and Cr addition on microstructure and magnetic properties of amorphous and nanocrystalline $Fe_{86-x}M_xZr_7Nb_2Cu_1B_4$ (M = Co, Ni, CoCr, and Cr, x = 0 or 6) alloys

Agnieszka Łukiewska, Jan Świerczek, Mariusz Hasiak, Jacek Olszewski, Józef Zbroszczyk, Piotr Gębara, Wanda Ciurzyńska

Abstract. Mössbauer spectra and thermomagnetic curves for the $Fe_{86-x}M_xZr_7Nb_2Cu_1B_4$ (M = Co, Ni, CoCr, and Cr, x = 0 or 6) alloys in the as-quenched state and after the accumulative annealing in the temperature range 600–800 K for 10 min are investigated. The parent $Fe_{86}Zr_7Nb_2Cu_1B_4$ amorphous alloy is paramagnetic at room temperature, and substitution of 6 at.% of Fe by Co, Ni, and CoCr changes the magnetic structure – the alloys become ferromagnetic, whereas replacing 6 at.% of Fe with Cr preserves the paramagnetic state. After the heat treatment at 600 K, the decrease of the average hyperfine field induction, as compared to the as-quenched state, is observed due to the invar effect. After this annealing, the Curie temperature for all investigated alloys decreases. The accumulative annealing up to 800 K leads to the partial crystallization; α-Fe or α-FeCo grains with diameters in the range of 12–30 nm in the residual amorphous matrix appear.

Key words: amorphous materials • nanocrystalline materials • Mössbauer spectroscopy • invar effect • Curie temperature

A. Łukiewska✉, J. Świerczek, J. Olszewski, J. Zbroszczyk, P. Gębara, W. Ciurzyńska
Institute of Physics,
Czestochowa University of Technology,
19 Armii Krajowej Ave., 42-200 Częstochowa, Poland,
Tel.: +48 34 325 0795, Fax: +48 34 325 0795,
E-mail: aluk@wip.pcz.pl

M. Hasiak
Institute of Materials Science & Applied Mechanics,
Wrocław University of Technology,
25 Smoluchowskiego Str., 50-370 Wrocław, Poland

Received: 18 June 2014
Accepted: 7 November 2014

Introduction

Fe-Zr-based amorphous alloys are a group of materials with both soft magnetic properties and anomalous magnetic behavior, such as spin glass and invar effects [1]. Owing to the lack of long-range order of atoms in amorphous materials, the exchange interaction between magnetic moment fluctuates, which involves inhomogeneity of the local magnetization. In materials containing, except for iron, additional transition metals, different magnetic moments of elements and chemical disorder lead to further exchange fluctuation. Since the exchange interaction between the magnetic moments depends on the atomic distance, competition between ferro- and antiferromagnetic interactions in amorphous alloys may occur [2]. Due to rapid quenching, free volumes are created in amorphous alloys, which enable modification of their magnetic properties in a very wide range by proper annealing. The structure relaxations occurring during this heat treatment cause atomic rearrangement and decrease of quenched-in free volumes in the amorphous materials. The controlled annealing allows us to obtain a partially crystallized amorphous precursor consisting of nanocrystalline grains dispersed in the amorphous matrix [3]. The intergranular matrix is usually highly inhomogeneous and has two components: the amorphous phase and the interface between crystalline grains and amorphous matrix may be distinguished [4]. The origin of ferromagnetism in the nanocrystalline alloys results from exchange coupling between

nanograins through the residual matrix. Mössbauer spectroscopy is an excellent method for studying the microstructure, magnetic order, and magnetization inhomogeneity of both amorphous and nanocrystalline materials.

Studying the effects of partial replacement of Fe with M = Co, Ni, CoCr, and Cr on the microstructure, magnetic order, and Curie temperature of $Fe_{86-x}M_xZr_7Nb_2Cu_1B_4$ (x = 0 or 6) alloys in the as-quenched state and after annealing is the purpose of this article.

Experimental procedure

Master $Fe_{86-x}M_xZr_7Nb_2Cu_1B_4$ (M = Co, Ni, CoCr, and Cr, x = 0 or 6) alloys were prepared by arc melting under an argon atmosphere using high-purity elements. Amorphous ribbons 3 mm wide and about 20 μm thick were produced by the melt spinning technique on the copper wheel in a protective argon atmosphere. The amorphicity of the as-quenched ribbons was checked by X-ray diffractometry and Mössbauer spectroscopy. A Bruker-AXS, type D8 Advanced X-ray diffractometer was used. From the X-ray diffraction profiles of partially crystallized samples the average diameter of the grains was determined using the Scherrer method [5]. A Mössbauer spectrometer was also used for the microstructure studies of the annealed samples. The transmission Mössbauer spectra were recorded at room temperature using a conventional constant acceleration spectrometer with a $^{57}Co(Rh)$ source of 50 mCi radioactivity, which enables us to measure recoil free emission and absorption of γ-rays by ^{57}Fe nuclei. The spectra were analyzed by a Normos package according to the procedure developed in Ref. [6]. Taking into account the symmetry of the X-ray patterns and the values of the hyperfine field induction of corresponding components [5, 7] the composition of the crystalline phases occurring in the investigated samples was determined. The Curie temperatures were obtained by the derivation of thermomagnetic curves recorded by means of a vibration sample magnetometer in the temperature range from 50 K up to 400 K in the magnetic field induction of 5 mT. Specific magnetization was measured for amorphous as-quenched samples and those annealed below the crystallization temperature. The specimens were subjected to the accumulative heat treatment in the temperature range from 600 K up to 800 K in a vacuum of 1.33×10^{-3} Pa. The annealing time at each temperature was equal to 10 min.

Results and discussion

Figure 1 shows X-ray diffraction patterns of the as-quenched samples. In the diffraction patterns, there is no evidence of any sharp peaks, and only broad maxima characteristic of the amorphous materials are present. Transmission Mössbauer spectra recorded at room temperature and corresponding probability distributions of the hyperfine field parameters for all investigated alloys in the as-quenched state are presented in Fig. 2. The master $Fe_{86}Zr_7Nb_2Cu_1B_4$ alloy is paramagnetic and its spectrum has the form of an asymmetric doublet. After

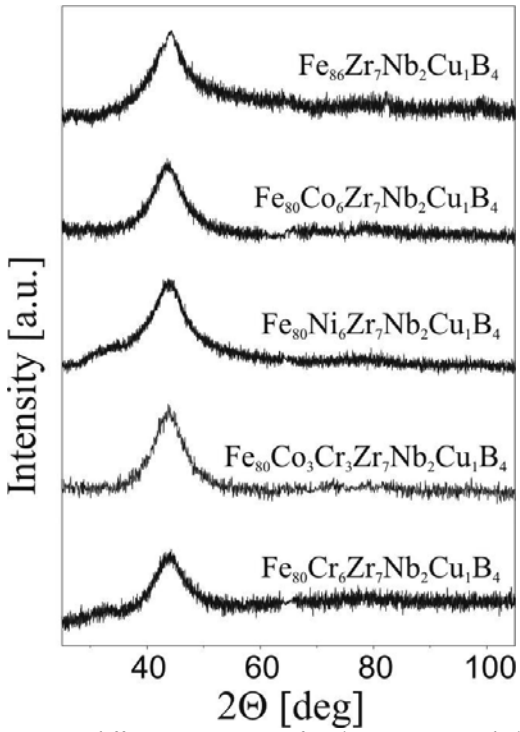

Fig. 1. X-ray diffraction patterns for the investigated alloys in the as-quenched state.

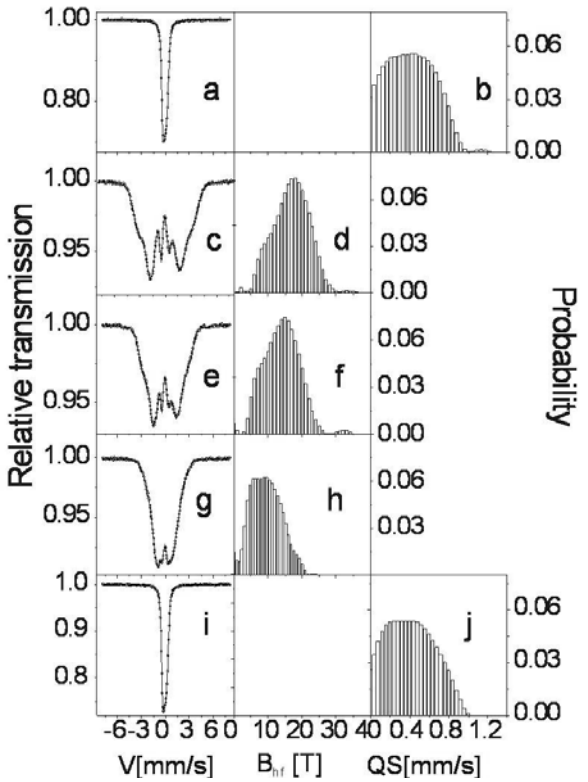

Fig. 2. Transmission Mössbauer spectra (a, c, e, g, and i) and corresponding probability distributions of quadrupole splitting (b and j) and hyperfine field induction (d, f, and h) for $Fe_{86-x}M_xZr_7Nb_2Cu_1B_4$ [M = Co (c and d), Ni (e and f), CoCr (g and h), and Cr (i and j), x = 0 (a and b) or 6 (c–j)] alloys in the as-quenched state.

replacement of 6 at.% of Fe with Co, Ni, and CrCo, the alloys become ferromagnetic at room temperature. The Mössbauer spectra of these alloys are typical of amorphous ferromagnets and consist of broad and overlapped lines [8]. However, substitution of 6 at.% of Fe by Cr preserves the paramagnetic state of the parent alloy. The probability distributions of the quadrupole splitting P(QS) for the paramagnetic alloys (Fig. 2b,j) exhibit a not-vanishing probability for QS = 0, indicating the existence of Fe sites with cubic symmetry of the atoms arranged in the nearest neighborhood, which give the zero value of the electric field gradient [9]. The probability distributions of the hyperfine field induction for the ferromagnetic alloys (Fig. 2d,f,h) exhibit bimodal characteristics with low- and high-field components. It is noteworthy that in the case of $Fe_{80}Ni_6Zr_7Nb_2Cu_1B_4$ (Fig. 2f) and $Fe_{80}Co_3Cr_3Zr_7Nb_2Cu_1B_4$ (Fig. 2h) amorphous alloys, the not-vanishing probability for $B_{hf} = 0$ is observed. In contrast to the paramagnetic materials, this fact cannot be ambiguously ascribed to the Fe sites with the cubic symmetry of the atoms arrangement, because pure quadrupole interactions should also be considered [9]. As compared to the as-cast state (Fig. 2a), only very small changes in Mössbauer spectra of the $Fe_{86}Zr_7Nb_2Cu_1B_4$ alloy are observed after the accumulative annealing up to 750 K (Fig. 3c). The spectra in the paramagnetic state are decomposed into a single line, and QS distribution exhibits also bimodal characteristics (Fig. 3, Table 1A). After the additional annealing at 755 K for 10 min, the ferromagnetic component with hyperfine field induction distribution appears with the most pronounced probability in the vicinity of B_{hf} = 33 T (Fig. 3f'). With the increase of the annealing temperature, the ferromagnetic component contribution increases (Fig. 3g,h,h'). After the last step of the annealing at 800 K for 10 min (Fig. 3i,j), the sample is fully ferromagnetic and its Mössbauer spectrum is decomposed into three components corresponding to amorphous matrix, interfacial zone, and crystalline α-Fe phase (Table 1A) [6]. A similar behavior is observed for the $Fe_{80}Cr_6Zr_7Nb_2Cu_1B_4$ alloy (Table 1E).

In Fig. 4, the Mössbauer spectra with the corresponding probability distributions of the hyperfine field for the $Fe_{80}Co_6Zr_7Nb_2Cu_1B_4$ alloy in the as-quenched state and after the accumulative annealing are depicted. The spectra of the samples annealed at 600 and 700 K are similar to that for the as-quenched sample and are characteristic of the amorphous ferromagnetic state. Bimodal characteristics of the probability distributions for the hyperfine field induction are preserved after the annealing. The distinct shoulder (low-field component) at about 10 T and the main maximum at about 18 T (high-field component) are visible. Moreover, a small tail in the probability distributions of the hyperfine field induction at high field induction is present. The bimodal shape of the probability distributions for the hyperfine field induction indicates that in the samples, two differ-

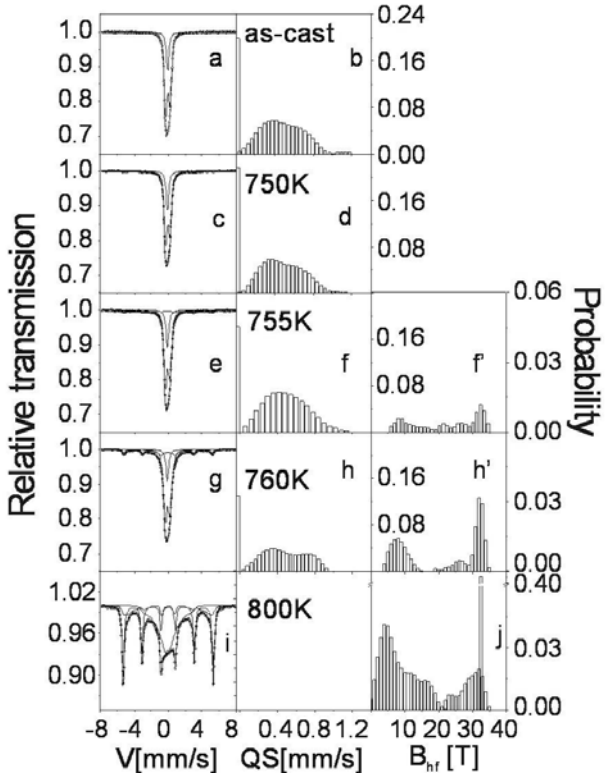

Fig. 3. Transmission Mössbauer spectra (a, c, e, g, and i) and corresponding probability distributions of quadrupole splitting (b, d, f, and h) and hyperfine field induction (f', h', and j) for the $Fe_{86}Zr_7Nb_2Cu_1B_4$ alloy in the as-quenched state and after the accumulative annealing for 10 min. The temperatures of the heat treatment are designated in the figure.

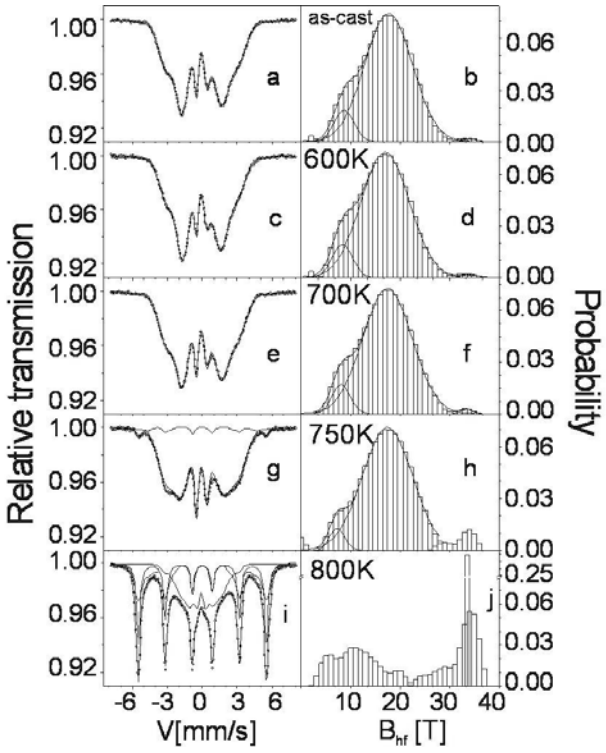

Fig. 4. Transmission Mössbauer spectra (a, c, e, g, and i) and corresponding probability distributions of hyperfine field induction (b, d, f, h, and j) for the $Fe_{80}Co_6Zr_7Nb_2Cu_1B_4$ alloy in the as-quenched state and after the accumulative annealing for 10 min. The temperatures of the heat treatment are designated in the figure.

Table 1. The average value of the hyperfine field induction for the amorphous phase ($\bar{B}_{am}$) and its standard deviation (ΔB_{am}), the relative intensity of the amorphous ferromagnetic component (I_{amf}), the average value of quadrupole splitting ($\overline{QS}$) and its standard deviation (ΔQS), the relative intensity of the amorphous paramagnetic component (I_{amp}), the isomer shift of single line (IS_{sl}), the relative intensity of the single line (I_{sl}), hyperfine field induction of crystalline phases (B_{cr}), the relative intensity of the crystalline component (I_{cr}), the average value of hyperfine field induction for the interfacial zone ($\bar{B}_{int}$) and its standard deviation (ΔB_{int}), the relative intensity of the interfacial component (I_{int}), and the Curie temperature (T_C) of the as-quenched and annealed alloys. Statistical uncertainties for the significant figure are given in brackets

	Alloys	Thermal history of the sample	$\bar{B}_{am}$ [T]	ΔB_{am} [T]	I_{amf}	$\overline{QS}$ [mm/s]	ΔQS [mm/s]	I_{amp}	IS_{sl} [mm/s]	I_{sl}	B_{cr} [T]	I_{cr}	$\bar{B}_{int}$ [T]	ΔB_{int} [T]	I_{int}	T_C [K]
		As-cast				0.485(2)	0.211(3)	0.80	–0.077(2)	0.20						278
		600 K				0.478(1)	0.205(1)	0.80	–0.087(1)	0.20						272
		700 K				0.483(4)	0.200(2)	0.79	–0.087(1)	0.21						273
A	$Fe_{86}Zr_7Nb_2B_4Cu_1$	750 K				0.494(1)	0.206(2)	0.81	–0.089(2)	0.19						
		755 K	22.40(5)	9.70(3)	0.100	0.509(2)	0.237(2)	0.72	–0.090(2)	0.18						
		760 K	21.40(2)	11.50(1)	0.220	0.583(5)	0.318(6)	0.65	–0.098(1)	0.13						
		800 K	8.20(2)	5.20(2)	0.420						33.02(5)	0.43	29.2(3)	3.4(2)	0.15	
		As-cast	16.90(4)	5.54(6)												420
		600 K	16.22(4)	5.57(6)												396
		700 K	16.83(4)	5.80(6)												402
B	$Fe_{80}Co_6Zr_7Nb_2B_4Cu_1$	750 K	16.53(5)	5.34(5)	0.940											
			32.34(5)	2.60(5)	0.060											
		800 K	11.10(2)	4.70(2)	0.360						34.1(1)	0.32	32.4(2)	3.4(3)	0.32	
		As-cast	14.23(4)	5.25(6)	0.986				–0.709(9)	0.014						374
		600 K	12.66(5)	5.04(9)	0.980				–0.0638(9)	0.02						359
C	$Fe_{80}Ni_6Zr_7Nb_2B_4Cu_1$	700 K	14.10(4)	5.41(6)	0.980				–0.105(7)	0.02						360
		750 K	11.30(1)	4.24(8)	0.460				0.092(2)	0.02	32.85(2)	0.17	22.0(2)	6.5(1)	0.35	
		800 K	7.70(5)	4.30(7)	0.220						33.13(4)	0.49	30.2(3)	3.5(3)	0.29	
		As-cast	9.27(2)	4.29(3)	0.975				–0.0961(5)	0.025						339
		600 K	9.12(3)	4.16(4)	0.972				–0.0808(6)	0.028						326
D	$Fe_{80}Co_3Cr_3Zr_7Nb_2B_4Cu_1$	700 K	9.34(4)	4.37(9)	0.972				–0.093(7)	0.028						330
		750 K	9.60(4)	4.84(9)	0.971				–0.101(4)	0.029						
		800 K	7.20(2)	4.70(2)	0.390				–0.118(4)	0.003	33.94(8)	0.17	31.0(2)	3.4(2)	0.41	
		As-cast				0.473(1)	0.205(2)	0.82	–0.118(2)	0.18						263
		600 K				0.464(7)	0.205(9)	0.83	–0.117(1)	0.17						253
E	$Fe_{80}Cr_6Zr_7Nb_2B_4Cu_1$	700 K				0.458(9)	0.189 2)	0.80	0.121(2)	0.20						256
		750 K				0.468(8)	0.195(1)	0.79	–0.129(1)	0.21						
		800 K				0.481(1)	0.319(2)	0.57			33.53(2)	0.11	26.1(2)	8.6(1)	0.32	

ent sites of Fe atoms are present [10]. The regions rich in iron and small distance between Fe atoms correspond to the low-field component, whereas the high-field component may be ascribed to the regions where Fe atoms in their neighborhood apart from Fe ones have other atoms. In the spectrum of the sample annealed at 750 K, the additional sextet of broad Lorentzian lines appears, resulting in the tail of the $P(B_{hf})$ at about 33 T (Fig. 4g,h; Table 1B). Moreover, the contribution of the low-field component in the probability distribution of the hyperfine field induction decreases. This behavior is associated with the early stage of the crystallization. The increase of the annealing temperature up to 800 K causes the appearance of the crystalline α-FeCo grains in the intergranular phase, which consists of two components: the amorphous matrix and interfacial zone (Fig. 4i,j; Table 1B).

In Fig. 5, the Mössbauer spectra, their decompositions, and probability distributions of the hyperfine field induction for the as-quenched and annealed $Fe_{80}Co_3Cr_3Zr_7Nb_2Cu_1B_4$ alloy are depicted. The values of hyperfine parameters are displayed in Table 1D. Replacing 3 at.% of Co with Cr leads to the distinct narrowing of the resulting spectra. In the corresponding probability distributions of the hyperfine field induction, two Gaussian components can be distinguished. The low-field component reaches its maximum after annealing at 600 K for 10 min. Although, as mentioned earlier, the origin of the not-vanishing probability for $B_{hf} = 0$ cannot be unambiguously prescribed, good results are obtained assuming the contribution of the single line.

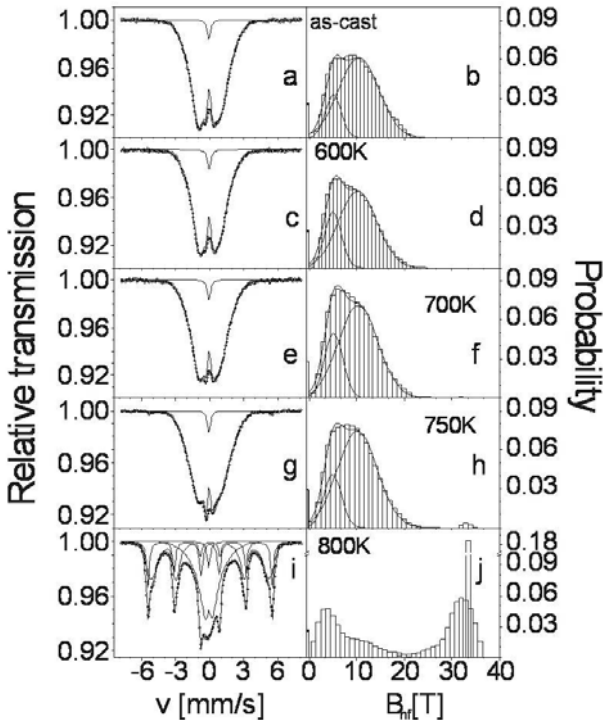

Fig. 5. Transmission Mössbauer spectra (a, c, e, g, and i) and corresponding probability distributions of hyperfine field induction (b, d, f, h and j) for the $Fe_{80}Co_3Cr_3Zr_7Nb_2Cu_1B_4$ alloy in the as-quenched state and after the accumulative annealing for 10 min. The temperatures of the heat treatment are designated in the figure.

Thus, the Mössbauer spectrum of this amorphous alloy can be presented as a superposition of one Lorentzian line and series of sextets corresponding to the distribution of the hyperfine field induction. The Mössbauer spectrum of the sample after the last step of annealing (800 K) was decomposed into three components: one corresponding to the amorphous matrix (described as a superposition of a single line and series of sextets corresponding to the distribution of the hyperfine field induction), the second ascribed to the interfacial zone (series of sextets), and the third attributed to the crystalline α-FeCo phase (singular sextet). A similar behavior is observed for the Ni-containing alloy (Table 1C). From Table 1 it is seen that for all ferromagnetic alloys the average value of the hyperfine field induction decreases after the annealing of the samples at 600 K and then 700 K for 10 min, due to the invar effect, and is slightly lower than that in the as-quenched state. This effect is the most pronounced for the $Fe_{80}Ni_6Zr_7Nb_2Cu_1B_4$ alloy. The observed phenomenon is associated with the annealing out of the free volumes during heat treatment of the amorphous samples, which leads to the decrease of the inter-atomic distance between magnetic atoms and in turn weakens the exchange interactions between them [11, 12]. It is in agreement with the increase of the low-field component in the $P(B_{hf})$ distributions. It is worth pointing out that 6 at.% of Co does not destroy the invar effect. After the last step of the annealing (800 K), the samples of all investigated alloys consist of nanograins with the diameter in the range 12–30 nm embedded in the highly inhomogeneous intergranular phase (Figs. 3–5).

As an example, in Fig. 6, specific magnetization at the magnetizing field induction of 5 mT vs. temperature in the range 50–400 K for the $Fe_{80}Co_3Cr_3Zr_7Nb_2Cu_1B_4$ alloy in the as-quenched state and after the annealing is shown. To obtain the Curie point, the derivative $d\sigma/dT$ is numerically calculated and presented as an inset in Fig. 6. The derived Curie temperatures are listed in Table 1 and are in agreement with the values of the hyperfine field induction. The decrease of the average B_{hf} is

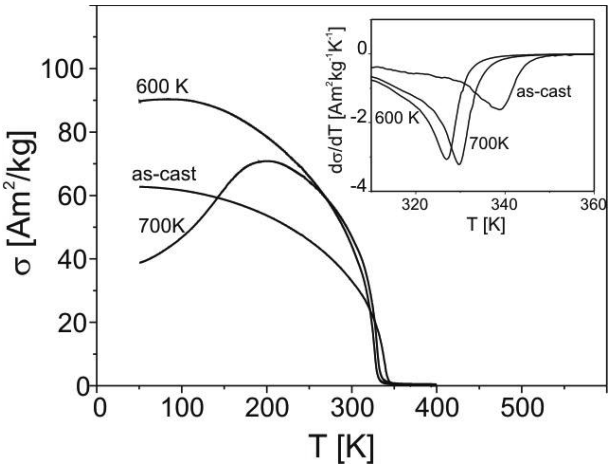

Fig. 6. Specific magnetization (σ), measured in the magnetizing field $B = 5$ mT and the derivative ($d\sigma/dT$) vs. temperature for the $Fe_{80}Co_3Cr_3Zr_7Nb_2Cu_1B_4$ alloy in the as-quenched state and after annealing at 600 K and then 700 K for 10 min.

accompanied by the decrease of Curie temperature because both depend on the exchange interactions. In the paramagnetic alloys at room temperature, that is, $Fe_{86}Zr_7Nb_2Cu_1B_4$ and $Fe_{80}Cr_6Zr_7Nb_2Cu_1B_4$, the decrease of the Curie temperature on annealing also takes place. One should expect that the appropriate changes in B_{hf} occur at a temperature lower than the ambient temperature.

Conclusions

- Replacing 6 at.% of Fe with Co, CoCr, Ni, and Cr influences distinctly the magnetic structure of the parent paramagnetic amorphous $Fe_{86}Zr_7Nb_2Cu_1B_4$ alloy. The Co-, CoCr- and Ni-containing alloys are ferromagnetic in the as-quenched state at room temperature, whereas the Cr-containing alloy is paramagnetic as confirmed by Mössbauer studies.
- The average hyperfine field induction and Curie temperature decrease after the annealing of $Fe_{80}Co_6Zr_7Nb_2Cu_1B_4$, $Fe_{80}Ni_6Zr_7Nb_2Cu_1B_4$, and $Fe_{80}Co_3Cr_3Zr_7Nb_2Cu_1B_4$ alloys at 600 K for 10 min.
- After the accumulative annealing at 800 K, the crystalline α-Fe or α-FeCo phases appear in the amorphous remainder, and the latter becomes poorer in iron than the parent alloy.

Acknowledgments. The authors would like to thank Dr hab. Piotr Pawlik for X-ray diffraction measurements.

References

1. Tange, H., Matsuyama, T., Chikazawa, A., Konishi, K., & Kamimori, T. (1998). Spin glass and Invar effect for Fe(ZrB) amorphous alloys. *J. Magn. Magn. Mater*., *177/181*, 125–126. DOI: 10.1016/S0304-8853(97)00505-2.
2. Ghafari, M., Chmielek, N., Keune, W., & Foley, C. P. (1989). Local magnetic properties of iron-rich amorphous $Fe_{100-x}Zr_x$ alloys. *Physica B*, *161*, 222–224. DOI: 10.1016/0921-4526(89)90138-5.
3. Mc Henry, M. E., Willard, M. A, & Laughlin, D. E. (1999). Amorphous and nanocrystalline materials for applications as soft magnets. *Prog. Mater. Sci.*, *44*, 291–433. DOI: 10.1016/S0079-6425(99)00002-X.
4. Ślawska-Waniewska, A., & Greneche, J. M. (1997). Magnetic interfaces in Fe-based nanocrystalline alloys determined by Mössbauer spectrometry. *Phys. Rev. B*, *56*, R8491–R8494. DOI: 10.1103/PhysRevB.56.R8491.
5. Cullity, B. D., & Stock, S. R. (2001). *Elements of X-ray diffraction* (3rd ed.). Prentice-Hall Inc.
6. Miglierini, M., & Greneche, J. M. (1997). Mössbauer spectrometry of Fe(Cu)MB-type nanocrystalline alloys: I. The fitting model for the Mössbauer spectra. *J. Phys.-Condens. Matter*, *9*, 2303–2319. DOI: 10.1088/0953-8984/9/10/017.
7. Frąckowiak, J. E. (1985). Determination of the long-range order parameter in the transition metal alloys using Mössbauer spectroscopy. *Phys. Status Solidi A-Appl. Mat.*, *87*, 109–119. DOI: 10.1002/pssa.2210870108.
8. Olszewski, J., Zbroszczyk, J., Fukunaga, H., Ciurzyńska, W., Łukiewska, A., Piasecki, M., Brągiel, P., Perduta, K., Młyńczyk, A., Lelątko, J. (2002). Transformation from amorphous to nanocrystalline state in $Fe_{85.4}Zr_{6.8-x}Nb_xB_{6.8}Cu_1$ (x = 0; 1) alloys. *J. Magn. Magn. Mater*., *241*, 381–389.
9. Świerczek, J. (2010). Medium range ordering and some magnetic properties of amorphous $Fe_{90}Zr_7B_3$ alloy. *J. Magn. Magn. Mater*., *322*, 2696–2702. DOI: 10.1016/j.jmmm.2010.04.010.
10. Olszewski, J., Zbroszczyk, J., Fukunaga, H., Ciurzyńska, W., Świerczek, J., Hasiak, M., Perduta, K., Łukiewska, A., & Młyńczyk, A. (2004). Microstructure studies of amorphous and nanocrystalline $(Fe_{1-x}Co_x)_{85.4}Zr_{6.8-y}M_yB_{6.8}Cu_1$ (x = 0 or 0.1, y = 0 or 1, M = Mo, Nb or Nd) alloys. *Nukleonika*, *49*(Suppl. 3), S79−S83. DOI: BUJ6-0006-0018.
11. Gondro, J., Świerczek, J., Rzącki, J., Ciurzyńska, W., Olszewski, J., Zbroszczyk, J., Błoch, K., Osyra, M., & Łukiewska, A. (2013). Invar behaviour of NANOPERM-type amorphous Fe-(Pt)-Zr-Nb-Cu-B alloys. *J. Magn. Magn. Mater*., *341*, 100–107, and references therein. DOI: 10.1016/j.jmmm.2013.04.009.
12. Coey, J. M. D. (1985). Magnetism in amorphous solid. *Amorphous Solid and Liquid State*, *13*, 433–466 DOI: 10.1007/978-1-4757-9156-3_13.